J. Fluid Mech. (2008), *vol.* 598, *pp.* 361–372.
doi:10.1017/S0022112008000189 Printed in the United Kingdom

Experimental investigation of homogeneity, isotropy, and circulation of the velocity field in buoyancy-driven turbulence

QUAN ZHOU, CHAO SUN AND KE-QING XIA

Department of Physics, The Chinese University of Hong Kong, Shatin, Hong Kong, China

(Received 15 October 2007 and in revised form 10 December 2007)

We present direct multipoint velocity measurements of the two-dimensional velocity field in the central region of turbulent Rayleigh–Bénard convection. The local homogeneity and isotropy of the velocity field are tested using a number of criteria and are found to hold to an excellent degree. The properties of velocity circulation Γ_r are also studied. The results show that the circulation appears to be more effective in capturing the effect of local anisotropy than the velocity field itself. The distribution of Γ_r is found to depend on the scale r, reflecting strong intermittency. It is further found that the velocity circulation has the same anomalous scaling exponents as the longitudinal and transverse structure functions for low-order moments ($p \lesssim 5$), whereas, for high-order moments ($p \gtrsim 5$), the anomalous scaling exponents for circulation are found to be systematically smaller than the scaling exponents of the longitudinal and transverse structure functions.

1. Introduction

An important issue in the study of fluid turbulence is to find the universal or quasi-universal properties of small-scale turbulence. A well-known quantity that may be used to characterize these properties is the velocity structure function (SF),

$$S_p(r) = \langle |V(\boldsymbol{x}+\boldsymbol{r}) - V(\boldsymbol{x})|^p \rangle, \tag{1.1}$$

where $V(\boldsymbol{x})$ is one of the components of the velocity vector at position $\boldsymbol{x}$, and $\boldsymbol{r}$ is the separation vector. When $\boldsymbol{r}$ is in the direction of $V(\boldsymbol{x})$, we have $S_p^L(r)$, the so-called longitudinal velocity structure function (LSF), while the transverse velocity structure function (TSF), $S_p^T(r)$, is obtained if the direction of $V(\boldsymbol{x})$ is perpendicular to $\boldsymbol{r}$. Assuming a scale-independent dissipation rate of the turbulent energy, Kolmogorov (1941) (K41) proposed that for homogenous and isotropic turbulence the velocity SFs scale as $S_p(r) \sim r^{\zeta_p} = r^{p/3}$ in the inertial range $\eta \ll r \ll L$, where η is the Kolmogorov scale characterizing the dissipative scale of the motion and L is the scale of energy injection. However, anomalous scaling, a nonlinear p-dependence of ζ_p, was later observed experimentally, and has been attributed to the so-called intermittency effect.

Another quantity, which can also be used to characterize the cascades in small-scale turbulence, is the velocity circulation, defined as

$$\Gamma_A = \oint_C \boldsymbol{V} \cdot \mathrm{d}\boldsymbol{\ell} = \int_A \boldsymbol{\omega} \cdot \mathrm{d}\boldsymbol{A}, \tag{1.2}$$

where A is a plane region enclosed by the contour C, $\mathrm{d}\boldsymbol{\ell}$ is the line element along the contour C and $\boldsymbol{\omega} = \nabla \times \boldsymbol{V}$ is the vorticity field. Here, a square region with side

length r is chosen and thus Γ_A can be considered equal to Γ_r without ambiguity. If the circulation is Gaussian distributed, meaning it has no intermittency, then the circulation structure function (CSF) should scale as $G_p(r) = \langle |\Gamma_r|^p \rangle \sim r^{4p/3}$, according to K41 arguments. However, in the real situation the existence of intermittency also leads to anomalous scaling. On the other hand, since Γ_r is an accumulation of the vorticity over a square region A, the velocity circulation is an ideal quantity to study both velocity and vorticity in small-scale turbulence as well as useful to study the spatial structures of vortex dynamics. In fact, from dimensional analysis it can be shown (Sreenivasan, Juneja & Suri 1995) that

$$G_p(r) \sim S_p^T(r) r^p. \tag{1.3}$$

Equation (1.3) implies that velocity circulation would have the same degree of intermittency with transverse velocity increment. There have been a limited number of studies on the scaling properties of velocity circulation. Sreenivasan *et al.* (1995) experimentally measured the velocity circulation in moderate-Reynolds-number turbulent wakes and found that the scaling exponents of circulation are smaller than the expected SF exponents plus p. Cao, Chen & Sreenivasan (1996) found numerically that the circulation is more intermittent than the longitudinal velocity increment, which suggests that there may exist a new class of anomaly. Separate numerical and experimental studies (Chen *et al.* 1997; Grossmann, Lohse & Reeh 1998; van der Water & Herweijer 1999) found that the TSFs are more intermittent than LSFs. Chen *et al.* (1997) further argued that two independent sets of exponents, one associated with the LSF and the other with the TSF (which may be related to CSF via (1.3), if it holds), may be required to describe the scaling of all small-scale features. In this scenario they conjectured that the LSF is related to the local energy dissipation ϵ_r and the TSF is related to the local enstrophy Ω_r, and the two sets of exponents correspond to different intermittency physics in fluid turbulence. On the other hand, using extended self-similarity analysis, Benzi *et al.* (1997) showed in a numerical turbulent shear flow that CSFs have the same anomalous contribution as the velocity SFs. It should be noted, however, that in the previous studies there has been no direct comparison between the CSF and TSF (LSF) experimentally measured from the same flow field. Therefore, how many independent scaling groups are needed to completely characterize all 'universal' features in small-scale turbulence remains an open question. From the point of view of validating various ideas and concepts in the studies of hydrodynamic turbulence, it is also important that these ideas and concepts should be tested in different types of turbulent flows, such as buoyancy-driven turbulence.

As an important class of turbulent flows, turbulent Rayleigh–Bénard convection (RBC), which is a fluid layer heated from below and cooled on the top, has been a well-controlled model system for studying buoyancy-driven turbulence and has attracted much attention during the past few decades (see, for example, Siggia 1994; Kadanoff 2001). Convective turbulence differs from other types of turbulent flows, such as turbulent shear flows and grid-generated turbulence, in many ways, but shares some common features with high-Reynolds-number turbulence, especially in the central region of the system where turbulent flow is far from the solid walls (plates and sidewalls) of the system and so the shear effect should be weak. In addition, the large-scale circulation is also concentrated near the perimeter of the cell and so its shear is also weak in the central region. As will be shown in this paper, as turbulent flow in the central region of RBC is approximately homogenous and isotropic, this system provides an ideal platform to study the general scaling properties of small-scale turbulence such as velocity circulation. Owing to the buoyancy effect, cascades

of velocity fluctuations in turbulent RBC are more complicated than those in non-buoyancy-driven turbulent systems, such as turbulent shear flows and grid-generated turbulence, and have been extensively studied in the past half century. Bolgiano (1959) and Obukho (1959, BO59) proposed that for stably stratified convection there is a length scale ℓ_B that divides the cascades of turbulent velocity and temperature fluctuations in the inertial range into two different dynamic regimes: above ℓ_B the buoyancy force is important and one expects the relation $S_p(r) \sim r^{3p/5}$; below ℓ_B the inertial force becomes dominant and one expects to observe the K41 scaling. Whether BO59 scaling exists in a turbulent Rayleigh–Bénard system has been a long-standing debate. In recent direct multipoint measurements of the velocity and temperature fields Sun, Zhou & Xia (2006) found that in the cell centre the velocity exhibits the same scaling behaviour as in homogeneous and isotropic Navier–Stokes turbulence, while in the vertical direction, near the sidewall, $S_p^L(r)$ is found to scale as $S_p^L(r) \sim r^{2p/5}$ plus intermittency corrections, which is neither BO59- nor K41-like behaviour and could be understood as a result of the coaction of buoyancy and inertial forces. Therefore, it appears that BO59 does not exist in the present range of Ra and Pr.

The remainder of this paper is organized as follows. We give detailed descriptions of the experimental setup in § 2 and present and analyse experimental results in § 3, which is divided into three parts. In §§ 3.1 and 3.2, we present several detailed tests and evidence, without invoking Taylor's hypothesis, to support a conclusion of Sun *et al.* (2006) that the convective flow in the central region of turbulent RBC is approximately locally homogenous and isotropic. In Sun *et al.* (2006), some of the evidence used to support this conclusion was simply given without showing how it was obtained. Section 3.3 discusses the scaling properties of velocity circulation. We summarize our findings and conclude in § 4.

2. Experimental setup and parameters

The multipoint velocity measurements were carried out in the centre of an RBC cell using the technique of particle image velocimetry (PIV). Both the cell and the technique have been described in detail in Sun, Xia & Tong (2005) and Sun *et al.* (2006) and thus we give only their main features here. The cell is a vertical cylinder of height $H = 19.3\,\mathrm{cm}$ and diameter $D = 19\,\mathrm{cm}$ (the aspect ratio is thus ~ 1). The top and bottom plates are made of copper with thickness 1 cm and gold-plated surfaces and the sidewall is made of 5 mm thick Plexiglas tube. Deionized and degassed water was used as convecting fluid. A square-shaped jacket made of flat glass plates and filled with water is fitted round the sidewall, which greatly reduced the distortion effect to the PIV images caused by the curvature of the cylindrical sidewall. During the measurements the convection cell was placed inside a thermostat box which was kept at the mean temperature (40°C) of the convecting fluid. In the PIV measurements, 50 μm diameter polyamid spheres (density $1.03\,\mathrm{g\,cm^{-3}}$) are used as seed particles and the laser lightsheet thickness is ∼0.5 mm. The spatial resolution of the velocity measurement is 0.66 mm, which is much smaller than the length scale of the lower end of the inertial range and hence is adequate to reveal the scaling properties in the inertial range, and the selected measuring area in the cell centre is $4 \times 4\,\mathrm{cm}^2$ (figure 1), corresponding to 61×61 velocity vectors. Denote the laser-illuminated plane as the (x, z)-plane, then the horizontal velocity component $u(x, z)$ and the vertical one $w(x, z)$ are measured.

The dynamics of the system depends on the Rayleigh number, defined as $Ra = \alpha g H^3 \Delta / \nu\kappa$, and the Prandtl number, defined as $Pr = \nu/\kappa$, where g is the

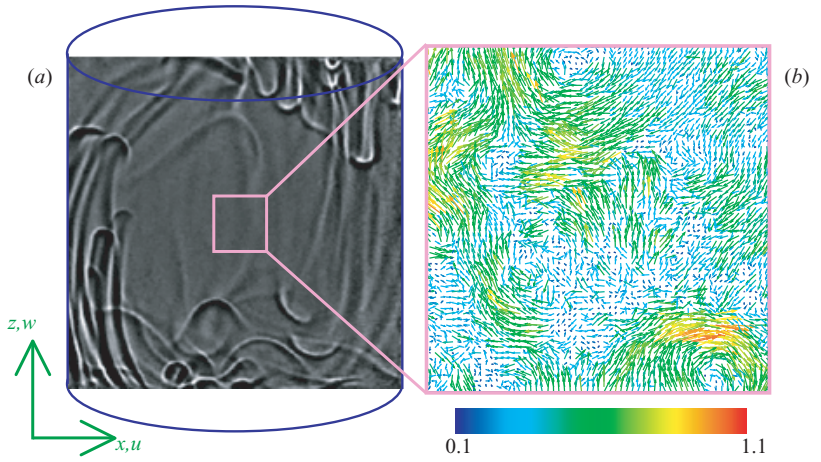

FIGURE 1. (*a*) Coordinate system and an example of a shadowgraph image showing the spatial distribution of thermal plumes in an aspect-ratio-one cell. The blue curves above and below the image illustrate the geometric shape of the convection cell. (*b*) An instantaneous vector map of the velocity field measured in the selected area shown in pink in (*a*).

acceleration due to gravity, Δ the temperature difference across the cell, and α, ν, and κ, respectively the thermal expansion coefficient, the kinematic viscosity, and the thermal diffusivity of the working fluid, which is water. The experiment was done at $Ra = 7.0 \times 10^9$ and $Pr = 4.3$. At these values, the global estimate of the Kolmogorov scale is $\eta = HPr^{1/2}/(RaNu)^{1/4} \approx 0.4\,\mathrm{mm}$ and that of the Bolgiano scale $\ell_B = HNu^{1/2}/(RaPr)^{1/4} \approx 5\,\mathrm{mm}$ (e.g. Cioni, Ciliberto & Sommeria 1995). The measurement lasted 1 hr, corresponding to an acquisition time of around 120 turnover times of the large-scale circulation. A total of 7500 vector maps were acquired with sampling frequency 2 Hz. Figure 1(*b*) shows a typical example of these vector maps.

3. Results

3.1. *Homogeneity*

High-order moment statistics of small-scale turbulence, such as velocity increments, usually needs a very large sample size to determine accurate temporal-averaged values. However, such a large sample is very difficult to acquire for multipoint velocity measurements, because of the limited sampling rate of the instruments. Nevertheless, if the flow is locally homogeneous, $S_p(r)$ and $G_p(r)$ are then independent of the position $\boldsymbol{x}$ and one may use spatial average instead of temporal average. The turbulent flow is locally homogenous if the N-point joint probability density function (PDF) of $\delta V_r = V(\boldsymbol{x}+\boldsymbol{r}) - V(\boldsymbol{x})$ for varying values of $\boldsymbol{r}$ is independent of $\boldsymbol{x}$ for every fixed N (Monin & Yaglom 1975). In Sun *et al.* (2006) we stated that the two-point and three-point joint PDFs are found to be independent of $\boldsymbol{x}$ and $\boldsymbol{r}$ without showing the actual results. In figure 2 these measured PDFs are shown for four different values of $\boldsymbol{x}$ for $u(x, z)$ and $w(x, z)$. All these PDFs collapse on top of each other, except some scatter near the tails which is probably due to the limited statistics (there are only 7500 samples for each velocity component). Thus, one may take the superposition of these PDFs as evidence for the approximate satisfaction of local homogeneity. Note also that the two-point PDFs have asymmetric tails with the positive tail being

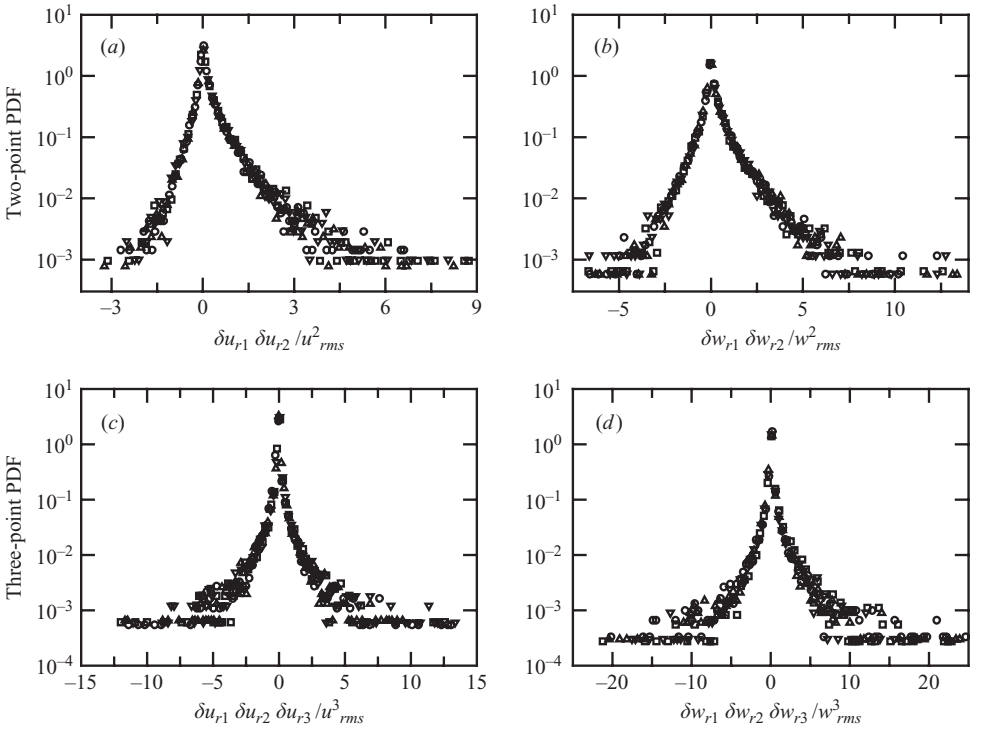

FIGURE 2. N-point joint PDFs for (a, c) $u(x, z)$ and (b, d) $w(x, z)$ with $N = 2$ (a, b) and $N = 3$ (c, d). Here $r1 = r3 = 25\eta$ and $r2 = 15\eta$. Four symbols (circles, squares, up-triangles and down-triangles) are used for four different values of $\boldsymbol{x}$.

larger than the negative one, which is due to the fact that there is certain degree of correlation between the velocity increments.

3.2. *Isotropy*

Isotropy is the central hypothesis for many theories and models of small-scale turbulence, such as the theory advanced by Kolmogorov (1941). For isotropic turbulence, the statistical properties of the flow are invariant with respect to rotations and reflections of the coordinate axes. The scaling properties of LSFs and TSFs in the central region of the cell and their comparison with other theoretical and experimental results have been reported and discussed in detail in Sun *et al.* (2006). Those results implied that the turbulent flow is approximately isotropic in the cell centre. Here, we present more evidence to support this conclusion. To the extent possible we follow the definitions of Sun *et al.* (2006) in the present paper, e.g. $S_p^{L,w}(r) = \langle |w(x, z + r) - w(x, z)|^p \rangle$ is defined as the pth-order LSF for w and its exponent is $\zeta_p^{L,w}$, etc.

Isotropy implies that when viewed from different directions, the values of LSFs or TSFs should be the same at some length scale r if the turbulent flow is locally isotropic at that scale. To check this, LSFs for two different (horizontal and vertical) directions of the order $p = 2$ and 4 are plotted in figure 3(a) and the corresponding TSFs are shown in figure 3(b); the structure functions are compensated by $(r/\eta)^{p/3}$ to increase the sensitivity of the test. The two arrows in figure 3 indicate the inertial range, which is operationally determined as the range of scales within which the

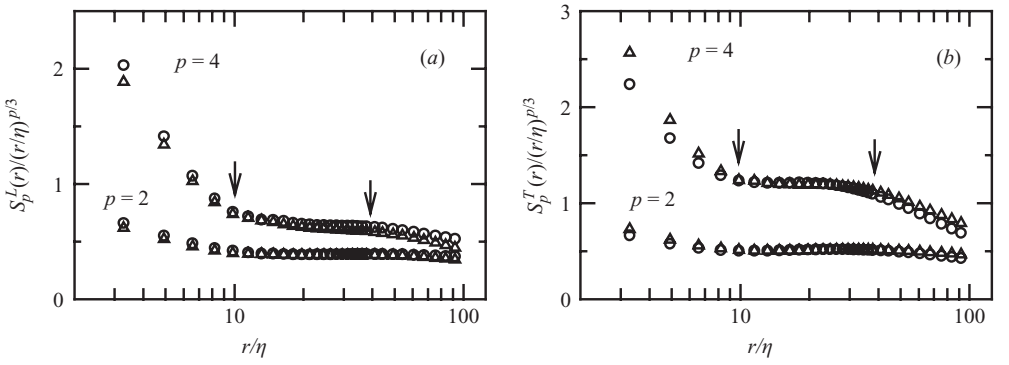

FIGURE 3. (*a*) LSFs $S_p^{L,w}(r)$ (triangles) and $S_p^{L,u}(r)$ (circles), and (*b*) TSFs $S_p^{T,w}(r)$ (triangles) and $S_p^{T,u}(r)$ (circles) normalized by $(r/\eta)^{p/3}$ as functions of r for $p = 2$ and 4. The two arrows indicate the inertial range.

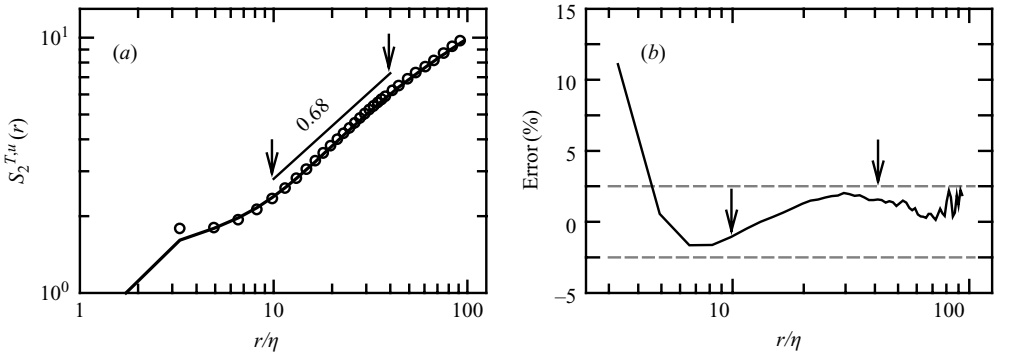

FIGURE 4. (*a*) A comparison of directly measured second-order TSF $S_2^{T,u}(r)$ (solid line) and that calculated from the second-order LSF $S_2^{L,u}(r)$ via (3.1) (circles). (*b*) The relative error between the two quantities plotted in (*a*).

third-order structure function exhibits power-law scaling. Coincidentally, the lower end of this range is around 10η. From figure 3 one sees that the compensated LSFs or TSFs of the same order for the x- and z-directions almost collapse onto each other in the inertial range. This is consistent with the instantaneous velocity field shown in figure 1(*b*) from which one cannot tell which direction is vertical and which is horizontal.

A simple but important and sensitive criterion for local isotropy is given by the following kinematic relationship between the second-order LSFs and TSFs (Monin & Yaglom 1975),

$$S_2^T(r) = S_2^L(r) + (r/2)\big(\partial S_2^L/\partial r\big), \tag{3.1}$$

since it is an invaluable and exact source of many known results. In Sun *et al.* (2006) we have shown that the above relationship holds approximately in an average sense over the inertial range. Here we make a more stringent test of the above functional relationship, i.e. the functions on each side should be the same for some scale r if the flow is isotropic at that scale. Figure 4(*a*) compares the directly measured second-order TSF (solid line) and the second-order TSF (circles) according to (3.1). The figure shows that (3.1) holds excellently not only in the inertial range but also for the largest values of r reached in the present measurements (note that the size of the measuring

area is much smaller than the system size). This can also be seen from figure 4(*b*) where the relative error between the directly measured TSF and that according to (3.1) are shown to be within 2.5% in the inertial range. Another criterion for local isotropy is that the cross-correlation function $C_z(r) = \langle w(x, y, z)u(x, y, z+r)\rangle / \sqrt{\langle w^2\rangle\langle u^2\rangle}$ between horizontal and vertical velocities vanishes in the inertial range (Monin & Yaglom 1975). Here, we find that in the inertial range $C_z(r)$, decreasing from 0.04 to 0.01, is indeed close to zero.

From the above results and discussion, we can conclude that the anisotropic effects in the inertial range are very weak for the central region of the turbulent RBC. This may be understood from the spatial distribution of thermal plumes, which has been found experimentally to be inhomogeneous in a closed cell (Qiu & Tong 2001; Shang *et al.* 2003, 2004). Figure 1(*a*) shows a typical example of a shadowgraph image (Xi, Lam & Xia 2004; the fluid dipropylene glycol, $Pr = 596$, is used because of its large shadowgraphic contrast compared with water) showing plumes' spatial distribution with warm plumes rising up one side of the cell (left side) and cold plumes falling down the other side of the cell (right side). The warm and cold plumes are separated laterally in the two opposing sidewall regions by the central core region and hence thermal plumes hardly appear in the central region. Since buoyancy force is exerted on the fluid mainly via thermal plumes, it is not surprising to find that the turbulence is nearly isotropic in the centre of the convection cell. Nevertheless we caution that the present measurements are only two-dimensional and made within the circulation plane of the large-scale circulation. Whether the velocity shows a different behaviour in planes with other orientations can only be answered by future three-dimensional measurements. It should also be noted that the present finding of a weak anisotropy is based on tests involving mostly low-order statistical moments of the velocity and a small amount of anisotropy may appear in higher-order statistical moments. To quantify the degree of anisotropy requires more sophisticated method such as the SO(3) group decomposition which may be used to disentangle systematically the isotropic and the anisotropic contributions by projecting the structure function of a given order over a particular spherical harmonic base (Arad, L'vov & Procaccia 1999*b*). This tool has been quite successful in quantifying the relative and absolute degrees of anisotropy of velocity fluctuations (Grossmann *et al.* 1998; Arad *et al.* 1998, 1999*a*; Kurien *et al.* 2000; Grossmann, von der Heydt & Lohse 2001) and in extracting anisotropic flow structures (Biferale *et al.* 2002). In turbulent convection the amount of anisotropy may be small in the central region but it may become significant near the boundaries. Regardless of the region of study, to separate and quantify the isotropic and the anisotropic parts of the flow field in this system, the SO(3) group decomposition method may have to be used in future studies.

3.3. *Velocity circulation*

The small-scale intermittency of the circulation fluctuations can be characterized by their distributions over different scales. The PDF for velocity circulation was first theoretically studied by Migdal (1994). Invoking the law of large numbers, he predicted that Γ_r should be Gaussian-distributed if r is large enough, such as in the inertial range. Sreenivasan *et al.* (1995) found that the PDF of Γ_r is close to Gaussian in the inertial range in moderate-Reynolds-number turbulent wakes. However, Cao *et al.* (1996) suggested that the arguments for Gaussianity based on the law of large numbers are questionable in the inertial range, because the circulation Γ_r consists of vorticity with all scales up to r. Then using the DNS data they showed that the PDF of Γ_r does depend on the area $A = r^2$ enclosed by the contour C, varying from the exponential distribution in the small scales (close to the dissipative scale) to the nearly

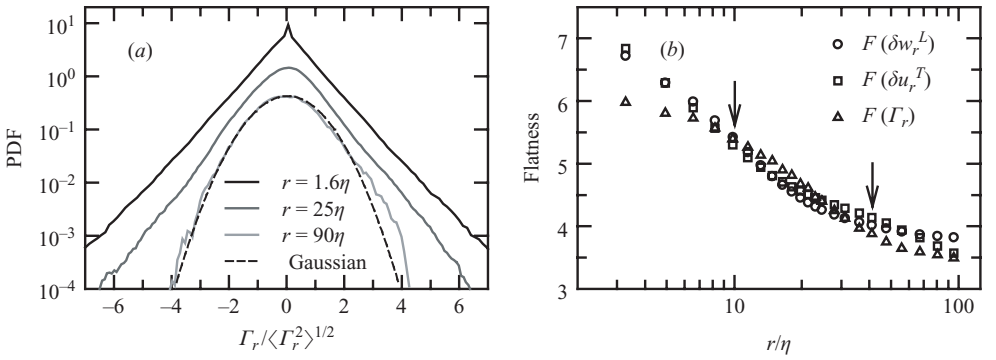

FIGURE 5. (*a*) PDFs of the velocity circulation Γ_r, from top to bottom, for $r = 1.6\eta$ (close to the dissipative scale), 25η (inertial range) and 90η (large scale). The PDFs have been shifted vertically for clarity. The dashed curve is a Gaussian fit to the PDF for $r = 90\eta$. (*b*) Flatness of the longitudinal velocity increment δw_r^L (circles), of the transverse velocity increment δu_r^T (squares) and of the circulation Γ_r (triangles) as functions of r.

Gaussian distribution in the large scales. Later, Benzi *et al.* (1997) reported the same results in a numerical study of turbulent shear flow. However, this scale-dependent distribution has not found experimental support so far.

In figure 5(*a*), we show experimentally measured PDFs of the circulation fluctuations for three different scales r, ranging from $r/\eta = 90$ (large scale), through 25 (typical inertial scale) down to 1.6 (close to dissipative scale). It is seen that the PDF clearly deviates from the Gaussian distribution when r is close to the dissipative scale ($r = 1.6\eta$) or in the inertial scale ($r = 25\eta$), and that it is approximately a Gaussian when r is close to the integral scale ($r = 90\eta$). This suggests that these PDFs depend on the scale r and are not self-similar, reflecting strong intermittency. A relatively sensitive measure of intermittency is given by the flatness. By definition, the flatness of a Gaussian-distributed quantity is 3. Figure 5(*b*) plots the measured flatness of the circulation $F(\Gamma_r) = \langle(\Gamma_r)^4\rangle/\langle(\Gamma_r)^2\rangle^2$ and those of the longitudinal and transverse velocity increments δw_r^L and δu_r^T. It is seen that all three flatnesses decrease with the scale r and are larger than the Gaussian value, especially in the inertial range. The figure also shows that, at the level of flatness, the three quantities, i.e. δw_r^L, δu_r^T and Γ_r have roughly the same degree of intermittency in the inertial range. This is in contrast to the finding by Cao *et al.* (1996) that the flatness of Γ_r is distinctly larger than that of the velocity increments.

Based on the properties of the measured flatness, one may expect that CSFs, LSFs and TSFs should have the same anomalous scaling exponents. To study the scaling behaviours of Γ_r, the CSFs G_p of order 1 to 8 are plotted as functions of r in figure 6(*a*), which are seen to exhibit nice power laws in the inertial range (between the two dashed lines). The local scaling exponents of order 1 to 4 are shown in figure 6(*b*), which are nearly constants in the inertial range. It is also noted that the scaling range exhibited by CSFs is larger and the qualities of the present power laws are better when compared with those of LSFs and TSFs. To examine the relationship between CSFs and TSFs, we note that if (1.3) is valid, the quantity $G_p(r)/[S_p^T(r)(r/\eta)^p]$ should then be independent of r. Figure 7(*a*) shows the log-log plot of $G_p(r)/[S_p^{T,u}(r)(r/\eta)^p]$ vs. r for $p = 1$ to 8. In the inertial range, the slopes of power-law fits for $p \leqslant 5$ are 0.02, 0.03, 0.06, 0.05 and −0.09, which are very close to the value of 0, while the slopes for $p > 5$ deviate from 0 markedly. Note that if $G_p(r) \sim r^{\chi_p}$ and $S_p^T(r) \sim r^{\zeta_p^T}$ in the

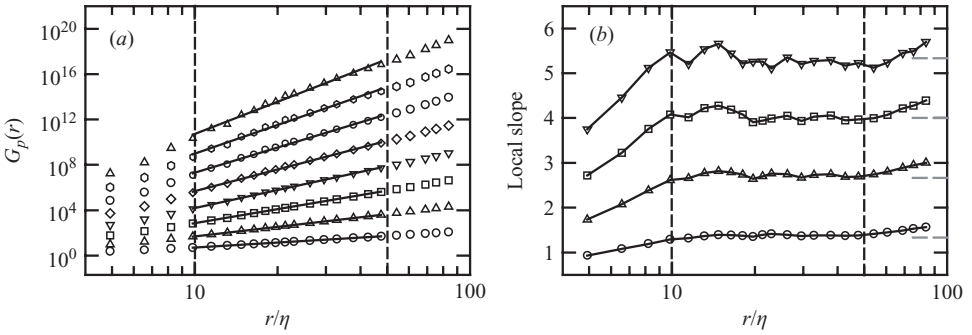

FIGURE 6. (*a*) CSFs $G_p(r)$ of order 1 to 8 (from bottom to top) as functions of r. The straight lines correspond to the best-fit to the data in the inertial range. (*b*) The local slopes of CSFs for $p = 1$ to 4, from bottom to top. The horizontal dashed lines near the right-hand axis indicate the corresponding K41 values. The vertical dashed lines indicate the inertial range.

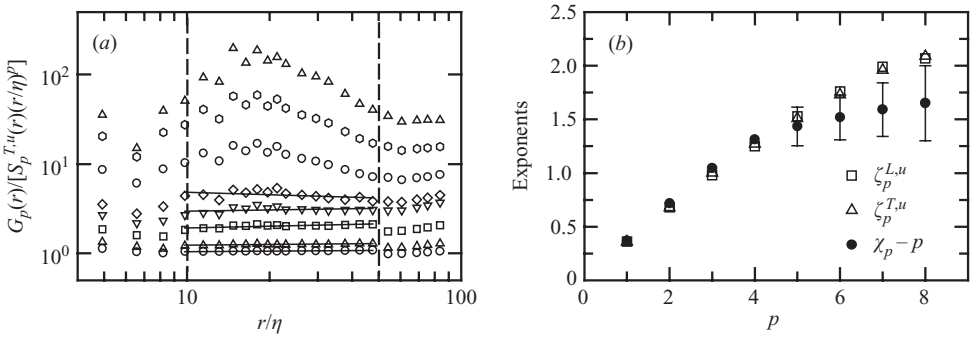

FIGURE 7. (*a*) Plots of $G_p(r)$, normalized by $S_p^{T,u}(r)(r/\eta)^p$, vs. r in log-log scale for $p = 1$ to 8, from bottom to top. The straight lines correspond to the best-fit to data in the inertial range. (*b*) Scaling exponents $\chi_p - p$ (solid circles) as a function of the moment order, p, compared with $\zeta_p^{L,u}$ (open squares) and $\zeta_p^{T,u}$ (open triangles). Typical error bars are shown for the highest four moments.

inertial range, then (1.3) also implies that $\chi_p = \zeta_p^T + p$. Figure 7(*b*) shows the scaling exponents $\chi_p - p$ as a function of the moment order, p, compared with $\zeta_p^{L,u}$ and $\zeta_p^{T,u}$. The figure shows that at the present level of sensitivity the circulation does not exhibit a different anomalous scaling from both longitudinal and transverse velocity increments for low-order moments ($p \lesssim 5$). This result is consistent with the result of Benzi *et al.* (1997), who found that the anomalous components of the velocity circulation and the velocity structure functions are equal (however, the highest p reached in their work is 6). Note that our result is a direct and stronger test of (1.3), while Benzi *et al.* used an indirect extended self-similarity method in their analysis due to the lack of a clear scaling for both CSF and SF. For high-order moments ($p \gtrsim 5$), however, $\chi_p - p$ is systematically smaller than the exponents of TSFs and LSFs, indicating a departure from (1.3).

To understand the differences between the exponents of CSFs and those of LSFs and TSFs for high-order moments, we examine the integration kernel $\Gamma_r^p P(\Gamma_r)$ of $G_p(r)$, which is shown in figure 8 for $p = 6$ and $p = 8$. First, the figure shows that the CSFs exhibit very good convergence even for $p = 8$. The figure also shows that

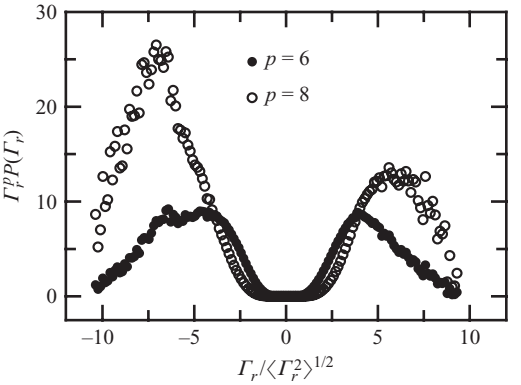

FIGURE 8. Integral kernels of CSF near the lower end ($r \simeq 10\eta$) of the inertial range for $p = 6$ (solid circles) and 8 (open circles). The vertical scale for $p = 8$ has been reduced by 15 for clarity.

$\Gamma_r^p P(\Gamma_r)$ is very asymmetric for $p = 8$ (for $p = 6$ there is already a small kink on the left peak). This is in sharp contrast to the velocity increments (see figure 1 of Sun *et al.* 2006); there it is shown that the integration kernels for TSFs are quite symmetric. Symmetry of the integration kernel also implies isotropy (at least in two opposite directions). Therefore, it appears that the CSFs are able to capture anisotropic effects more effectively than SFs, though these effects are very weak in our case. It has also been argued previously that circulation is more sensitive to coherent structures like filaments (plumes in the present case) than structure functions, which are one-dimensional cuts of three-dimensional turbulence (Sreenivasan *et al.* 1995). Note that (1.3) is based on dimensional arguments and mathematically it implies that the CSF and TSF have the same distribution and hence the same degree of intermittency. But in fact, as circulation is an area integration of transverse velocity increments, the presence of intermittency and/or correlation among transverse velocity increments may invalidate (1.3). Therefore the departure from (1.3) could be due to two factors: one is intermittency and the other is that CSF is more effective in capturing coherent objects that are also anisotropic, as discussed above. The fact that the CSF exponents are different from the SF exponents only for larger p is probably because both of the above two factors are usually manifested as the non-Gaussian tails in the PDFs (exponential-like tails for intermittency and asymmetric tails for small-scale anisotropy) that are captured better by the high-order moments.

4. Conclusions

In summary, we have experimentally measured the two-dimensional velocity field in the central region of turbulent RBC and investigated the scaling features of velocity circulation without invoking Taylor's hypothesis. The local homogeneity and local isotropy of the velocity are tested based on various criteria and, to an excellent approximation, these properties are found to hold in the central region of turbulent thermal convection. To our knowledge, few such experimental tests exist for any type of turbulent flows, whether they are buoyancy-driven or not. Our results also show that the circulation is more sensitive to local anisotropy than the velocity field itself. By directly comparing CSFs with LSFs and TSFs measured in the same velocity field, our results show that for low-order statistics ($p \lesssim 5$) no significant differences beyond

experimental uncertainty are found among their corresponding scaling exponents. However, for high-order statistics ($p \gtrsim 5$), the anomalous scaling exponents of CSFs become systematically smaller than those of LSFs and TSFs. This suggests that it is possible that a new intermittency physics different from that for velocity increments is required for circulation, which is manifested only in high-order statistics. Thus, the question of whether velocity circulation has different anomalous scaling than the velocity increments remains open. Clearly, further experimental and numerical studies at higher Ra (Re) and higher-resolution are needed to settle this issue.

We thank R. Benzi for stimulating discussions and acknowledge support of this work by the Research Grants Council of Hong Kong SAR under Grant Nos. CUHK 403705 and 403806.

REFERENCES

Arad, I., Biferale, L., Mazzitelli, I. & Procaccia, I. 1999*a* Disentangling scaling properties in anisotropic and inhomogeneous turbulence. *Phys. Rev. Lett.* **82**, 5040–5043.

Arad, I., Dhruva, B., Kurien, S., L'vov, V. S., Procaccia, I. & Sreenivasan, K. R. 1998 Extraction of anisotropic contributions in turbulent flows. *Phys. Rev. Lett.* **81**, 5330–5333.

Arad, I., L'vov, V. S. & Procaccia, I. 1999*b* Correlation functions in isotropic and anisotropic turbulence: The role of the symmetry group. *Phys. Rev.* E **59**, 6753–6765.

Benzi, R., Biferale, L., Struglia, M. V. & Tripiccione, R. 1997 Self-scaling properties of velocity circulation in shear flows. *Phys. Rev.* E **55**, 3739–3742.

Biferale, L., Lohse, D., Mazzitelli, I. & Toschi, F. 2002 Probing structures in channel flow through SO(3) and SO(2) decomposition. *J. Fluid Mech.* **452**, 39–59.

Bolgiano, R. 1959 Turbulent spectra in a stably stratified atmosphere. *J. Geophys. Res.* **64**, 2226–2229.

Cao, N., Chen, S. & Sreenivasan, K. R. 1996 Properties of velocity circulation in three-dimensional turbulence. *Phys. Rev. Lett.* **76**, 616–619.

Chen, S., Sreenivasan, K. R., Nelkin, M. & Cao, N. 1997 Refined similarity hypothesis for transverse structure functions in fluid turbulence. *Phys. Rev. Lett.* **79**, 2253–2256.

Cioni, S., Ciliberto, S. & Sommeria, J. 1995 Temperature structure functions in turbulent convection at low Prandtl number. *Europhys. Lett.* **32**, 413–418.

Grossmann, S., von der Heydt, A. & Lohse, D. 1997 Scaling exponents in weakly anisotropic turbulence from the Navier-Stokes equation. *J. Fluid Mech.* **440**, 381–390.

Grossmann, S., Lohse, D. & Reeh, A. 1997 Different intermittency for longitudinal and transversal turbulent fluctuations. *Phys. Fluids* **9**, 3817–3825.

Grossmann, S., Lohse, D. & Reeh, A. 1998 Scaling of the irreducible SO(3)-invariants of velocity correlations in turbulence. *J. Statist. Phys.* **93**, 715–724.

Kadanoff, L. P. 2001 Turbulent heat flow: Structures and scaling. *Phys. Today* **54(8)**, 34–39.

Kolmogorov, A. N. 1941 The local structure of turbulence in incompressible viscous fluid for very large Reynolds numbers. *Dokl. Akad. Nauk. SSSR* **30**, 301–305.

Kurien, S., L'vov, V. S., Procaccia, I. & Sreenivasan, K. R. 2000 Scaling structure of the velocity statistics in atmospheric boundary layers. *Phys. Rev.* E **61**, 407–421.

Migdal, A. A. 1994 Loop equation and area law in turbulence. *Intl J. Mod. Phys.* A **9**, 1197–1238.

Monin, A. S. & Yaglom, A. M. 1975 *Statistical Fluid Mechanics*, vol. 2. MIT Press.

Obukhov, A. M. 1959 The influence of hydrostatic forces on the structure of the temperature field turbulent flow. *Dokl. Akad. Nauk. SSSR* **125**, 1246.

Qiu, X.-L. & Tong, P. 2001 Onset of coherent oscillations in turbulent Rayleigh-Bénard convection. *Phys. Rev. Lett.* **87**, 094501.

Shang, X.-D., Qiu, X.-L., Tong, P. & Xia, K.-Q. 2003 Measured local heat transport in turbulent Rayleigh-Bénard convection. *Phys. Rev. Lett.* **90**, 074501.

Shang, X.-D., Qiu, X.-L., Tong, P. & Xia, K.-Q. 2004 Measurements of the local convective heat flux in turbulent Rayleigh-Bénard convection. *Phys. Rev.* E **70**, 026308.

Siggia, E. D. 1994 High Rayleigh number convection. *Annu. Rev. Fluid Mech.* **26**, 137–168.

Sreenivasan, K. R., Juneja, A. & Suri, A. K. 1995 Scaling properties of circulation in moderate-Reynolds-number turbulent wakes. *Phys. Rev. Lett.* **75**, 433–436.

Sun, C., Xia, K.-Q. & Tong, P. 2005 Three-dimensional flow structures and dynamics of turbulent thermal convection in a cylindrical cell. *Phys. Rev.* E **72**, 026302.

Sun, C., Zhou, Q. & Xia, K.-Q. 2006 Cascades of velocity and temperature fluctuations in buoyancy-driven thermal turbulence. *Phys. Rev. Lett.* **97**, 144504.

van de Water, W. & Herweijer, J. A. 1999 High-order structure functions of turbulence. *J. Fluid Mech.* **387**, 3–37.

Xi, H.-D., Lam, S. & Xia, K.-Q. 2004 From laminar plumes to organized flows: the onset of large-scale circulation in turbulent thermal convection. *J. Fluid Mech.* **503**, 47–56.